Development of chromium ion substituted Zn-Co-Ca-Fe-Ba ferrites for energy storage applications

S. Knani [a], M. I. Arshad [b], M. S. Al-Buriahi [c], N. Amin [b], K. Mehmood [b], U. Kashif [b], M. Irfan [b], A. Nisar [b,*]
[a]*Center for Scientific Research and Entrepreneurship, Northern Border University, Arar 73213, Saudi Arabia*
[b]*Magnetic & Innovative Materials in Nanotechnology (MiMi Nanotech) Research Lab, Department of Physics, Government College University, Faisalabad, Pakistan 38000*
[c]*Department of Physics, Sakarya University, Sakarya, Turkey*

Ferrites are most extensively studied materials primarily due to their unique and diverse characteristics. Thus, chromium doped $Zn_{0.25}Co_{0.5}Ca_{0.25}Fe_{1.97}Ba_{0.03-y}Cr_yO_4$ (y = 0, 0.01, 0.02, 0.03) ferrites were easily and economically synthesized via a sol-gel auto combustion method, and their dielectric, magnetic and molecular vibrational were thoroughly characterized. The existence of three active molecular vibrational modes A_{1g}, T_{2g}, and E_g was verified by Raman spectroscopy. Frequency-dependent dielectric characteristics were measured using the LCR meter. The frequency range of 4 Hz to 8 MHz has been used to study the dielectric property. While ac conductivity shows an increasing trend with increasing frequency, capacitance and impedance decrease as frequency increases. This comparative analysis enables researchers to select materials suitable for energy storage applications, particularly lithium-ion batteries, based on their desired dielectric properties. Furthermore, the observed hysteresis loop revealed a decrease in retentivity (Mr), saturation magnetization (Ms), and coercive field (Hc).

(Received January 19, 2025; Accepted July 7, 2025)

Keywords: Sol-gel auto combustion method, Impedance, Chromium, AC conductivity

1. Introduction

Ferrite nanoparticles are widely used as distinction materials in magnetic memories, magnetic-resonance imaging, microwave equipment, and recording devices [1-2]. Metals oxides with magnetic characteristics, such as TFe_2O_4 (where T = Mg^{2+}, Cd^{2+}, Fe^{2+}, Cu^{2+}, Mn^{2+}, etc.), are essentially spinel ferrites. These materials that possess distinctive characteristics that render them appropriate for many applications, including drug-delivery systems, microwave absorbers, and gas sensors. Inside the cubic spinel structure, metal ions are trapped at both octahedral and tetrahedral interstices by the closely packed oxygen ions. For the formation of a normal spinel, divalent cations reside the tetrahedral interstices and trivalent cations reside in the octahedral interstices. An inverse spinel is produced half divalent cations occupy tetrahedral interstices, and the other divalent ions and trivalent ions occupy octahedral interstices [3-7].

Ferrite nanoparticles were synthesized using several Methods, including hydrothermal method,co-precipitation, ball milling, and sol gel auto-combustion techniques. Among these above methods, sol-gel chemical synthesis has several advantages over the others, including easy processing, cost effectiveness, homogenous reactant mixing, control over particle size and homogeneity of size distribution [8-10]. The exceptional features of cobalt ferrite including its strong magneto-crystalline anisotropy, low saturation magnetization, large coercivity, high magnetostrictive, significant chemical stability, and mechanical hardness, have drawn a lot of

* Corresponding author: ashagcuf8@gmail.com
https://doi.org/10.15251/JOR.2025.214.409

interest. Because of these characteristics, cobalt ferrite is now an ideal material for a wide range of technological applications [11].

Considering that calcium is naturally non-toxic, ferrite of calcium $CaFe_2O_4$ should be more biocompatible. But since a single ferrite cannot satisfy all requirements, magnetic nanocomposites combine the advantages of each phase. Hard magnetic barium hexaferrite $BaFe_{12}O_{19}$ is extensively utilized owing to its cost-effectiveness, superior oxidation and corrosion resistance, extremely low density, high electrical resistivity, elevated saturation magnetization, and substantial. Meanwhile, the spinel ferrite $CoFe_2O_4$ is an ideal soft ferrite characterized by significant anisotropy, strong saturation magnetization, and medium coercivity at room temperature [12].

Rare earth (RE) metal ions such as Gd^{3+}, Nd^{3+}, Sm^{3+}, Ho^{3+}, and Cr^{3+} can be substituted for cobalt ferrite to change its structural disorder, lattice strain, and other characteristics. Since iron contains 3d unpaired electrons and rare-earth elements have 4f unpaired electrons, the addition of RE^{3+} results in the RE^{3+} - Fe^{3+} interaction, which determines the electrical, spectral, structural, and magnetic characteristics. Furthermore, the properties of cobalt ferrite are influenced by the type of cation dispersion, particle size, ionic size, chemical compositions, and synthesis methods [13]. The large ionic radii of the RE elements might cause a shift in cell symmetry and consequently internal stress when cations are replaced with smaller ionic radii in different types of structures. Consequently, the dielectric, magnetic properties of substitution elements are altered as well as to the material's structural characteristics (such as an increased cell parameter and decreased average crystallite and grain diameters) [14-15].

Frequency-dependent ac conductivity measurements are beneficial techniques for describing transport process in spinel ferrite [16]. N. Sivakumar et al. used complex impedance spectroscopy to investigate the electrical characteristics of nanocrystalline $CoFe_2O_4$, and their findings indicate that the material's conductivity increased as grain size decreases. The ac conductivity of Co-Zn ferrite changes with temperature and composition, in the low frequency region [17].

This research work explains the dielectric, magnetic and vibrational characteristics of rare earth (Cr) doped Zn-Co-Ca-Ba spinel ferrite synthesized via Sol-gel auto combustion method. The review of the literature revealed that no research had been done on how Cr substitution affected the characteristics of Zn-Co-Ca-Ba ferrites made using the sol-gel auto-combustion process. In view of this, we investigate how Cr-substitution affects the real and imaginary part of impedance, and ac conductivity and vibrational modes of $Zn_{0.25}Co_{0.5}Ca_{0.25}Fe_{1.97}Ba_{0.03-y}Cr_yO_4$ (y=0.00, 0.01, 0.02, and 0.03) produced using the sol-gel auto-combustion process

2. Materials and methods

In this research work, Sol-gel auto combustion method was used to produce $Zn_{0.25}Co_{0.5}Ca_{0.25}Fe_{1.97}Ba_{0.03-y}Cr_yO_4$ (y= 0, 0.01, 0.02, 0.03). The chemicals used were Zinc (II) nitrate $Zn(NO_3)_2.6H_2O$, cobalt (II) nitrate $Co(NO_3)_2.6H_2O$, calcium (II) nitrate $Ca(NO_3)_2.6H_2O$, Iron (III) nitrate $Fe(NO_3)_3.9H_2O$, Barium (III) nitrate [$Ba(No_3)_2.6H_2O$], Chromium (III) nitrate [$Cr(NO_3)_2.6H_2O$], and citric acid ($C_6H_8O_7.H_2O$).An electronic balance was used to weight the needed amount of chemicals. The reagents were weighed in accordance with their stoichiometric ratios; metal nitrate and citric acid were added in a 1:1 ratio. We prepared aqueous nitrate solutions using distilled water. Before providing temperature carefully added an ammonium solution, adjusting the pH to a neutral level of approximately 7. Heating the solution to 100°C with a magnetic stirrer the solution was transformed into a gel-like state by evaporating the water, resulting in a dense, dry gel that spontaneously ignited, only ash left inside the beaker, then grinding to make a fine powder. All powders from these specimens were sintered at 800 ^{0}C for 5 hours to achieve the final ferrite products. Fig. 1 represents the complete process.

Impedance Analyzer (Model IM 3536 Hioki) was used to evaluate the dielectric properties at room temperature using Zn-Co-Ca-Ba-Cr spinel ferrite nanoparticle pellets in the frequency range of 4 Hz to 8MHz. The vibrational modes of synthesized Zn-Co-Ca-Ba-Cr ferrite

nanoparticles were studied using Confocal Micro Raman spectroscopy (MNSTEX PRI 100, DONGWOO, South Korea).

3. Result and discussion

3.1. Raman spectroscopy

The fig.2 displays the Raman spectrum for $Zn_{0.25}Co_{0.5}Ca_{0.25}Fe_{1.97}Ba_{0.03-y}Cr_yO_4$, ferrite with various Cr^{3+} ion concentration y, denoted by y = 0, 0.01, 0.02, 0.03, There are three Raman-active modes identified, A_{1g}, T_{2g}, and Eg.

The addition of Cr^{3+} ion results in a substantial positive frequency shift for all phonon modes when transition from Zn-Co-Ca-Ba ferrite to from Zn-Co-Ca-Ba-Cr ferrite, likely attributable to differences in the masses or radii of the ions at that site [18-19]. The E_g mode of molecular vibration, occurring between 334.28 and 338.07 cm^{-1}, belongs to the symmetric bending of O^{2-} at the octahedral site. However, the bands in the 476.72-485.99 cm^{-1} range are associated with T_{2g} symmetry, which results from O_2 expanding at octahedral locations. The A_{1g} mode originates from the symmetrical extensions of the O^{2-} ions adjacent to the Fe-O and Ni-O bonds in the tetrahedral sites. The Raman signals within the range of 650.69- 652.49 cm^{-1} belong to the A_{1g} modes, indicating the extension of vibrations of Fe^{3+} or O_2 ions at the A site. The cation movement in spinel ferrite occurs due to the transition of metal ions from the tetrahedral site to the octahedral site [20-23].

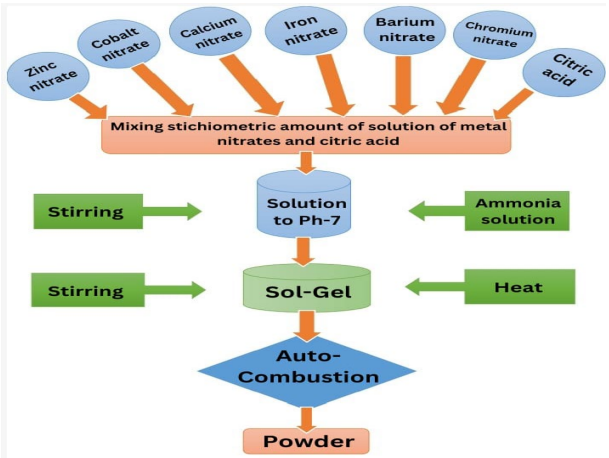

Fig. 1. Schematic diagram for the synthesis of spinel ferrite samples.

Table 1. Raman modes for Cr^{3+} doped Zn-Co-Ca-Ba ferrite samples.

y	Raman shift (cm^{-1})		
	E_g	T_{2g}	A_{1g}
	(B) Site	(B) Site	(A) Site
0.0	334.28	476.72	652.49
0.01	336.17	478.57	654.30
0.02	336.17	484.14	650.69
0.03	338.07	485.99	650.69

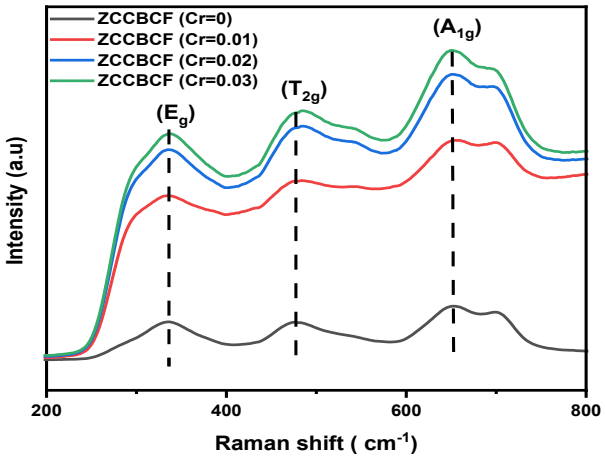

Fig. 2. Raman spectra for Cr^{3+} doped Zn-Co-Ca-Ba ferrite samples.

3.2. Dielectric analysis

The dielectric properties of synthesized ferrite were investigated using an LCR meter at room temperature having frequency range 4 Hz to 8 MHz. The resulting graphs revealed trends of increase or decrease in dielectric properties across various frequencies. The capacity of the capacitor is the when a potential difference passes across its plates, a capacitor's capacity to hold charge is known as its capacitance. The capacitance of $Zn_{0.25}Co_{0.5}Ca_{0.25}Fe_{1.97}Ba_{0.03-y}Cr_yO_4$ with y = 0, 0.01, 0.02, 0.03, and 1.0 was determined via LCR meter. Fig. 3 depicts how frequency f (Hz) affects capacitance.

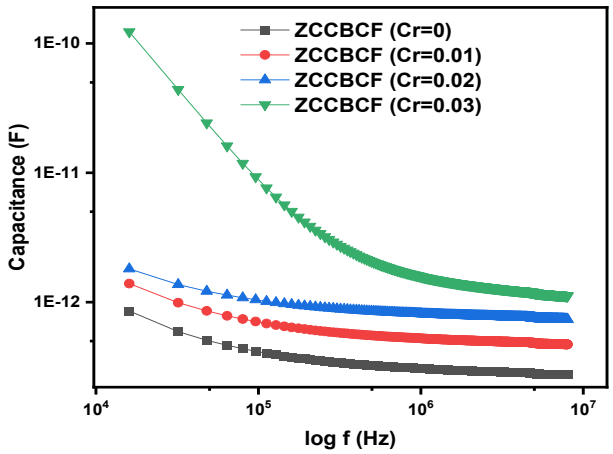

Fig. 3. Graph between capacitance and frequency Cr^{3+} doped Zn-Co-Ca-Ba ferrite samples.

At low frequency, Capacitance values are greater and exhibit decline as frequency increases. The frequency rises, the ac field flips so quickly and the dipoles as well as charge carriers have no sufficient time to flip with the applied ac-field, causing polarization to drop and, thus, the capacity to store charge to decrease. According to Koop's theory, the material's behavior at lower frequencies, grains behave like conductor, meanwhile grain boundaries behave like insulators. In the low frequency region, Charge carriers formed at grain boundaries, which raises interfacial polarization and increases the dielectric's storage capacity. At higher frequencies, charge carriers were unable to approach the grain boundaries, because of shorter relaxation time duration, preventing interfacial polarization and lowering the dielectric's capacitance. According to Fig. 3, the capacitance of pure ferrite is significantly lower than that of Zn-Co-Ca-Ba spinel

ferrites doped with chromium ions. Notably, a direct correlation is noticed among the concentration of chromium ions and capacitance, suggesting enhanced charge accumulation at the grain boundaries [24].

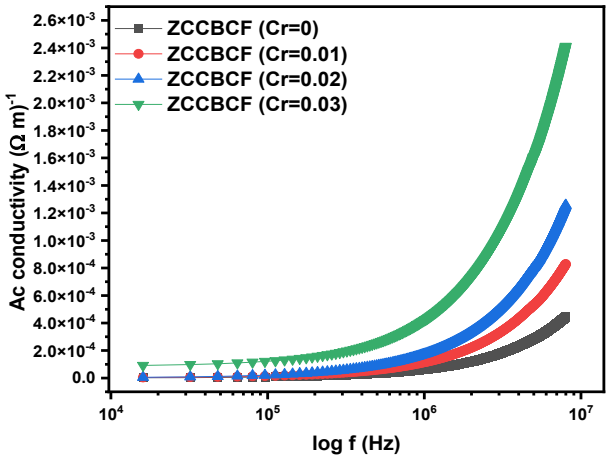

Fig. 4. Graph between Ac conductivity and frequency of Cr^{3+} doped Zn-Co-Ca-Ba ferrite samples.

The AC conductivity was calculated from dielectric constant (ε′) and dielectric loss tangent (tan δ) as

$$\sigma_{ac} = 2\pi f \varepsilon_o \varepsilon' Tan\delta$$

where $Tan\delta$ is the tangent loss factor, f is the frequency, "ε_o" is the permittivity of free space and "ε′" is the real part of the permittivity.

Fig. 4 shows the graph between the log of f and AC conductivity for prepared ferrites samples. Charge carriers migrate from grain boundaries rather than accumulate and cause polarization, which is known as the ac conductivity. At higher frequencies, conduction of charge carriers improves because of higher active grain. Conversely, insulating grain boundaries become more prominent at lower frequencies, leading to a decrease in AC conductivity. Therefore, compared to pure Zn-Co-Ca-Ba ferrite, the hopping charge carriers increased in the Zn-Co-Ca-Ba-Cr ferrite because of some freely bound charges, which improved the material's ac conductivity [25].

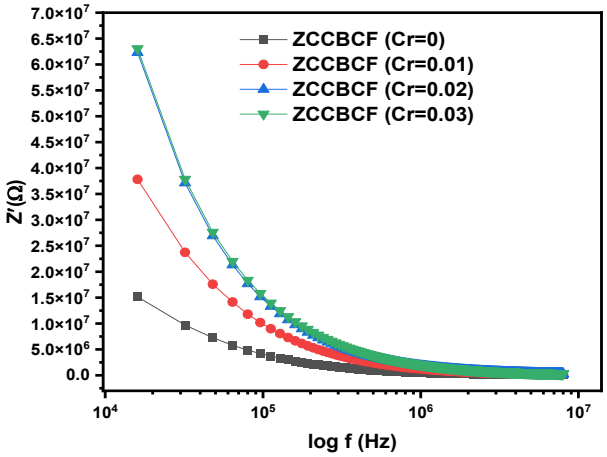

Fig. 5. Real part of Impedance versus frequency of $Cr3^{+}$ doped Zn-Co-Ca-Ba ferrite samples.

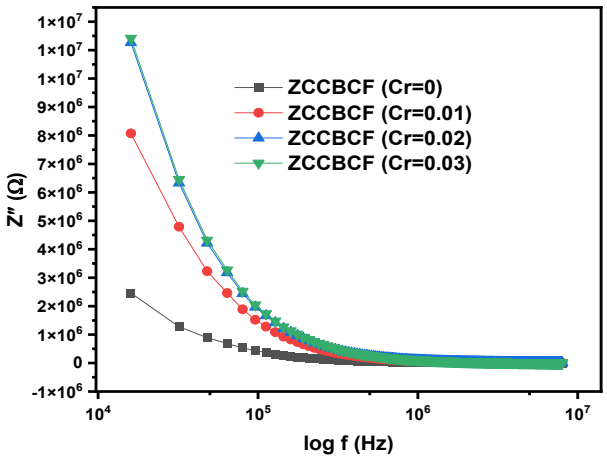

Fig. 6. Imaginary part of Impedance versus frequency of Cr^{3+} doped Zn-Co-Ca-Ba ferrite samples.

The electrical transport characteristics of spinel-type ferrites can be better understood using impedance analysis, which also provides information on the reactive (imaginary component, Z″) and resistive (real part, Z′) contributions to conductivity under AC field application. Fig.5 depicts that real component of impedance (Z') changes with frequency for $Zn_{0.25}Co_{0.5}Ca_{0.25}Fe_{1.97}Ba_{0.03-y}Cr_yO_4$ (y= 0, 0.01, 0.02, 0.03). As the frequency rises up to 0.1MHz, Z′ is shown decreasing before attainment of stable value. The decrease in Z′ as the frequency rises represents a decrease in the ac resistivity value [27]. At low frequency region, value of impedance has high value because the existences of space charge polarization in the sample. The impedance value becomes constant at 10^6Hz.

Nyquist plots between Z′ and Z" have been made to assess the contribution of bulk and inter grain boundaries to the conduction mechanism in Fig.7. While grains perform better at higher frequencies, grain boundaries are more prominent at lower frequencies. Greater density of imperfections observed in resistive inter-grain boundaries hinder charge carriers from passing when combined with the rapidly fluctuating AC field. Thus, where resistive grain boundaries are prevalent, charge carriers exhibit relaxation. At low frequency, resistive inter grain boundaries show as a semicircle. Semicircular arcs are used to represent conducting grains at high frequencies, particularly when the resistance values are low [28].

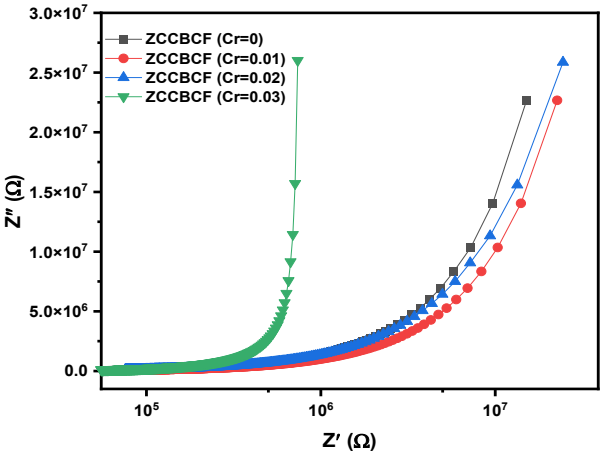

Fig. 7. Nyquist plots of Cr^{3+} doped Zn-Co-Ca-Ba ferrite samples.

3.3. Hysteresis loop analysis

Fig. 8 displays the M-H hysteresis loop for $Zn_{0.25}Co_{0.5}Ca_{0.25}Fe_{1.97}Ba_{0.03-y}Cr_yO_4$, ferrite with various Cr^{3+} ion concentration y, denoted by y = 0, 0.01, 0.02, recorded at room temperature. Magnetic characteristics like saturation magnetization, retentivity, coercive field, and squareness ratio (SQ) were determined using VSM data, as well as the findings are shown in Table 2. Table 2 indicates that an increase in the concentration of chromium ions inside the host matrix results in a decrease in the values of the magnetic parameters. The reason for this is the antiferromagnetic nature of chromium and the reduced spin magnetic dipole moment (μ) of Cr^{3+} (3.87 μB) in comparison to Fe^{3+} (5.91 μB).The magneto-crystalline anisotropic constant (K= $\frac{Hc \times Ms}{0.96}$) were evaluated and clearly shown in table 2. As the amount of chromium ions increases, the coercive field decreases from 768.9653 to 546.0884, which is caused by the decreasing anisotropy field, which also lowers the domain wall energy. A decrease in the squareness ratio (Mr/Ms) with increasing Cr content was observed. Microwave frequencies were investigated utilizing the relationship $\omega_m = 8\pi^2 M_s \gamma$, involving the gyromagnetic ratio (γ), which exhibited a value of 2.8 MHz/Oe. Table 2 presents the experimentally observed microwave operating frequencies, ranging from 13.77 GHz to 11.27 GHz. This suggests that the synthesized samples exhibit multidomain magnetic behavior. This attribute is essential for attaining soft magnetic characteristics, rendering them appropriate for use in high-frequency transformers, motors, inductors, and generators [29].

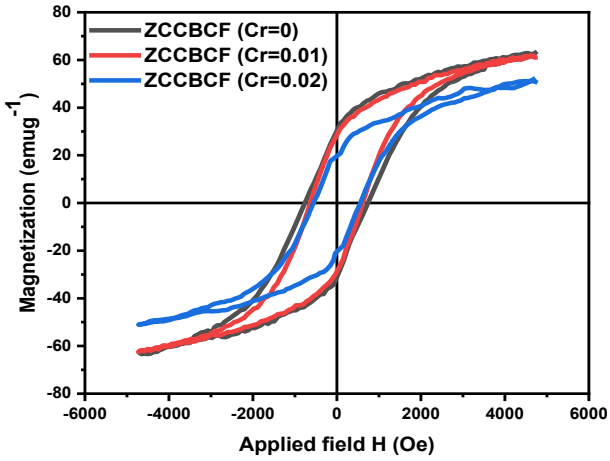

Fig. 8. Hysteresis loops for Cr^{3+} doped Zn-Co-Ca-Ba ferrite samples.

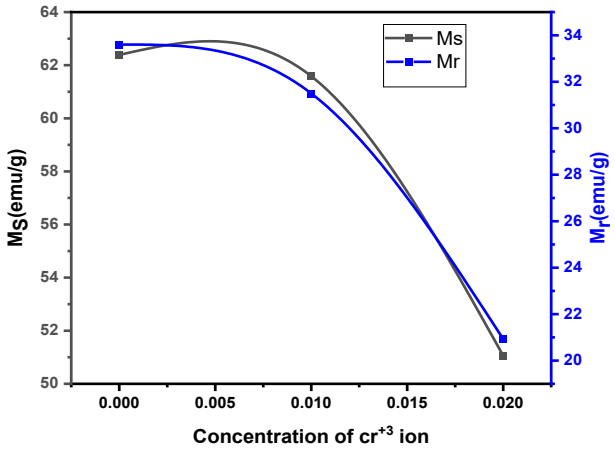

Fig. 9. Saturation magnetization and remanence vs concentration of Cr^{+3} for ferrite samples.

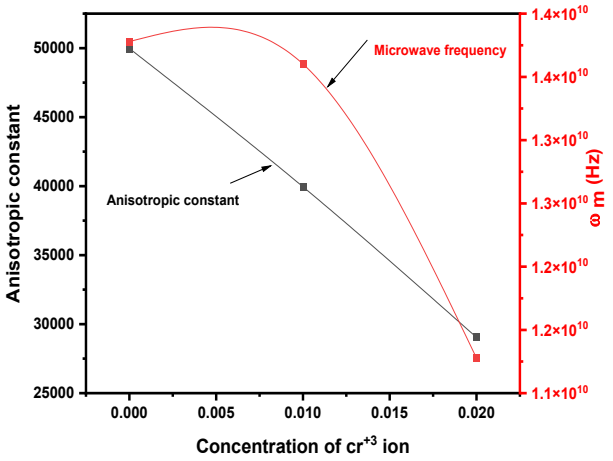

Fig. 10. Anisotropic constant and microwave frequency vs concentration of Cr^{+3} for ferrite samples.

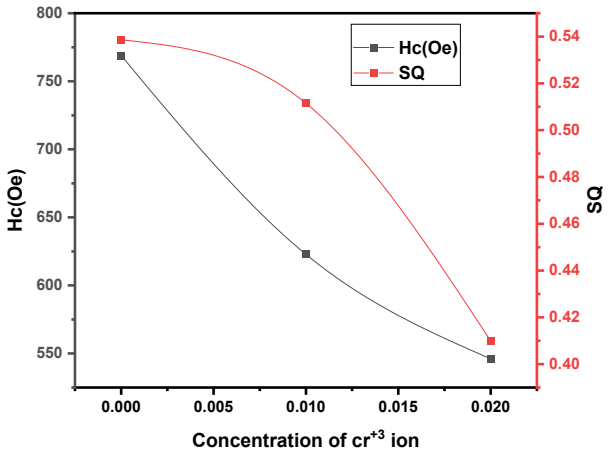

Fig. 11. Coercivity (Hc), and squareness ratio (SQ) vs concentration of Cr^{+3} for ferrite samples

Table 2. Magnetic parameters for Cr^{3+} doped Zn-Co-Ca-Ba ferrite samples.

Y	H_C (Oe)	SQ	M_r (emu/g)	M_s (emu/g)	K (erg/cm^3)	ω_m (GHz)
0.00	768.9653	0.53863	33.604	62.388	49973.13243	13.77
0.01	622.7781	0.5115	31.50	61.584	39951.21512	13.60
0.02	546.0884	0.40989	20.93	51.062	29046.21446	11.27

4. Conclusion

Cr^{3+} doped Zn-Co-Ca-Ba ferrites were fabricated through sol-gel auto combustion method. The existence of three active molecular vibrational modes A_{1g}, T_{2g}, and E_g was verified by Raman spectroscopy. The dielectric study indicated that capacitance and impedance reached their peak values in low-frequency range and declined with high frequency region due to interfacial polarization. The AC exhibited diminished values in the low-frequency zone as a result of increased activity at grain boundaries, whereas it improved with frequency due to the enhanced activity of conducting grains in the high-frequency regime. The results and analysis indicate that the increased capacitance, particularly ac-conductivity, provide these Cr^{3+} doped Zn-Co-Ca-Ba ferrite samples ideal candidates for energy storage devices. This resulted in a narrowing of the hysteresis loop, signifying an enhancement in soft magnetic characteristics.

Acknowledgments

The authors extend their appreciation to Northern Border University, Saudi Arabia, for supporting this work through project number (NBU-CRP-2025-2483).

References

[1] Hasan, I. H., Hamidon, M. N., Ismail, A., Ismail, I., Mohd Azhari, N. A., Mohd Kusaimi, M. A., Azhari, S. (2019), Materials Chemistry and Physics, 236; https://doi.org/10.1016/j.matchemphys.2019.121790
[2] Ozawa, E. (2019), IEEE Transactions on Magnetics, 55(7); https://doi.org/10.1109/TMAG.2019.2893652
[3] Mehmood, K., Rehman, A. U., Amin, N., Morley, N. A., Arshad, M. I. (2023), Journal of Alloys and Compounds, 930; https://doi.org/10.1016/j.jallcom.2022.167335
[4] Arshad, M. I., Dastgir, A., Alresheedi, F., Amin, N., Tung, L. D., Amami, M., Thi Kim Thanh, N., Zahid, H., Jacob, J., Ezzine, S., Rehman, A. U. (2024), Journal of Alloys and Compounds, 978; https://doi.org/10.1016/j.jallcom.2023.173015
[5] Majeed, M., Akhtar, M., Khatoon, R., Amin, N., Morley, N., Tung, L. D., Amami, M., Abbas, W., Siddeeg, S. M., Thi Kim Thanh, N., Sajjad, M. T., Arshad, M. I. (2024), Journal of Alloys and Compounds, 986; https://doi.org/10.1016/j.jallcom.2024.173770
[6] Khalid, M. U., Ajaz-un-Nabi, M., Arshad, M. I., Rehman, A. U., Hussain, K., Arshad, S., El-Bahy, Z. M., el Sayed, M. E., Amin, N. (2024), Ceramics International, 50(13), 24025–24035; https://doi.org/10.1016/j.ceramint.2024.04.134
[7] Aslam, A., Razzaq, A., Naz, S., Amin, N., Imran Arshad, M., Ajaz Un Nabi, M., Nawaz, A., Mahmood, K., Bibi, A., Iqbal, F., Shakil, M., Farooq, Z., Zahir Iqbal, M., Shabhi Haider, S., ur Rehman, A. (n.d.), Impact of Lanthanum-Doping on the Physical and Electrical Properties of Cobalt Ferrites; https://doi.org/10.1007/s10948-021-05802-4/Published
[8] Akhtar, M., Ur Rehman, A., Amin, N., Hussain, K., Imran Arshad, M. (2024), Journal of Magnetism and Magnetic Materials, 595; https://doi.org/10.1016/j.jmmm.2024.171831
[9] Latif, Z., Rehman, A. U., Yusuf, M., Amin, N., Arshad, M. I. (2022), Journal of Ovonic Research, 18(4), 627–635; https://doi.org/10.15251/JOR.2022.184.627
[10] Rehman, A. U., Sharif, S., Hegazy, H. H., Morley, N., Amin, N., Akhtar, M., Arshad, M. I., Farooq, Z., Munir, Z., Munir, T. (2023), Materials Today Communications, 34; https://doi.org/10.1016/j.mtcomm.2023.105371
[11] Latif, Z., Rehman, A. U., Amin, N., Arshad, M. I., Marzouki, R. (2023), RSC Advances, 13(49), 34308–34321; https://doi.org/10.1039/d3ra02080k
[12] Yang, H., Ye, T., Lin, Y., Zhu, J., Wang, F. (2016), Journal of Alloys and Compounds, 683, 567–574; https://doi.org/10.1016/j.jallcom.2016.05.127
[13] Arshad, M. I., Mehmood, K., Amin, N., Morley, N. A., Thanh, N. T. K. (2023), Composites Communications, 39; https://doi.org/10.1016/j.coco.2023.101571
[14] Aslam, A., Rehman, A. U., Amin, N., Ajaz un Nabi, M., Abdullah, Q. ul ain, Morley, N. A., Arshad, M. I., Ali, H. T., Yusuf, M., Latif, Z., Mehmood, K. (2021), Journal of Physics and Chemistry of Solids, 154; https://doi.org/10.1016/j.jpcs.2021.110080
[15] Bulai, G., Diamandescu, L., Dumitru, I., Gurlui, S., Feder, M., Caltun, O. F. (2015), Journal of Magnetism and Magnetic Materials, 390, 123–131; https://doi.org/10.1016/j.jmmm.2015.04.089
[16] Hankare, P. P., Sanadi, K. R., Garadkar, K. M., Patil, D. R., Mulla, I. S. (2013), Journal of Alloys and Compounds, 553, 383–388; https://doi.org/10.1016/j.jallcom.2012.11.181
[17] Sivakumar, N., Narayanasamy, A., Shinoda, K., Chinnasamy, C. N., Jeyadevan, B., Greneche, J. M. (2007), Journal of Applied Physics, 102(1); https://doi.org/10.1063/1.2752098
[18] Arshad, M. I., Hasan, M. S., Rehman, A. U., Amin, N., Tung, L. D., Kim Thanh, N. T., Morley, N. A., Amami, M., Alresheedi, F., Ezzine, S., Gadhi, M. A. (2024), Journal of Alloys and Compounds, 972; https://doi.org/10.1016/j.jallcom.2023.172847
[19] Saleem, M., Varshney, D. (2018), AIP Conference Proceedings, 1953; https://doi.org/10.1063/1.5032428

[20] Akhtar, M., Hasan, M. S., Amin, N., Morley, N. A., Arshad, M. I. (2024), Journal of Rare Earths, 42(1), 137–146; https://doi.org/10.1016/j.jre.2023.01.021
[21] Chavan, A. R., Somvanshi, S. B., Khirade, P. P., Jadhav, K. M. (2020), RSC Advances, 10(42), 25143–25154; https://doi.org/10.1039/d0ra04319b
[22] Arshad, M. I., Zahid, H., Sajjad, M. T., Tung, L. D., Amin, N., Thanh, N. T. K., Amami, M., Morley, N., Alresheedi, F., Dastgir, A., Siddeeg, S. M., Hasan, M. S. (2024), Powder Technology, 438; https://doi.org/10.1016/j.powtec.2024.119469
[23] Panda, S. S. S., Parne, S. R., Sharma, S., Gandi, S., Panigrahi, T. (2024), Journal of Sol-Gel Science and Technology; https://doi.org/10.1007/s10971-024-06419-4
[24] Mubasher, Mumtaz, M., Bashir, A., Rashid, M., Umar, T., Sarfraz, Z., Zia, H. (2022); Materials Innovations, 02(02), 36–46; https://doi.org/10.54738/mi.2022.2201
[25] Mubasher, Mumtaz, M., Hassan, M., Ali, L., Ahmad, Z., Imtiaz, M. A., Aamir, M. F., Rehman, A., Nadeem, K. (2020), Applied Physics A: Materials Science and Processing, 126(5); https://doi.org/10.1007/s00339-020-03529-y
[26] Assar, S. T., Abosheiasha, H. F. (2015), Journal of Magnetism and Magnetic Materials, 374, 264–272; https://doi.org/10.1016/j.jmmm.2014.08.011
[27] Hossain, M. D., Khan, M. N. I., Nahar, A., Ali, M. A., Matin, M. A., Hoque, S. M., Hakim, M. A., Jamil, A. T. M. K. (2020), Journal of Magnetism and Magnetic Materials, 497; https://doi.org/10.1016/j.jmmm.2019.165978
[28] Kamran, M., Anis-ur-Rehman, M. (2023), Materials Science in Semiconductor Processing, 153; https://doi.org/10.1016/j.mssp.2022.107111
[29] Senbeto, E. K., Elangovan, S. (2023), Journal of Nanomaterials, 2023; https://doi.org/10.1155/2023/5103278